AIP Journal of Applied Physics

Prospects of zero Schottky barrier height in a graphene-inserted MoS2-metal interface

Anuja Chanana and Santanu Mahapatra

Citation: Journal of Applied Physics **119**, 014303 (2016); doi: 10.1063/1.4938742
View online: http://dx.doi.org/10.1063/1.4938742
View Table of Contents: http://scitation.aip.org/content/aip/journal/jap/119/1?ver=pdfcov
Published by the AIP Publishing

JOURNAL OF APPLIED PHYSICS **119**, 014303 (2016)

Prospects of zero Schottky barrier height in a graphene-inserted MoS_2-metal interface

Anuja Chanana and Santanu Mahapatra
Nano-Scale Device Research Laboratory, Department of Electronic Systems Engineering, Indian Institute of Science (IISc) Bangalore, Bangalore 560012, India

(Received 29 October 2015; accepted 14 December 2015; published online 4 January 2016)

A low Schottky barrier height (SBH) at source/drain contact is essential for achieving high drive current in atomic layer MoS_2-channel-based field effect transistors. Approaches such as choosing metals with appropriate work functions and chemical doping are employed previously to improve the carrier injection from the contact electrodes to the channel and to mitigate the SBH between the MoS_2 and metal. Recent experiments demonstrate significant SBH reduction when graphene layer is inserted between metal slab (Ti and Ni) and MoS_2. However, the physical or chemical origin of this phenomenon is not yet clearly understood. In this work, density functional theory simulations are performed, employing pseudopotentials with very high basis sets to get insights of the charge transfer between metal and monolayer MoS_2 through the inserted graphene layer. Our atomistic simulations on 16 different interfaces involving five different metals (Ti, Ag, Ru, Au, and Pt) reveal that (i) such a decrease in SBH is not consistent among various metals, rather an increase in SBH is observed in case of Au and Pt; (ii) unlike MoS_2-metal interface, the projected dispersion of MoS_2 remains preserved in any MoS_2-graphene-metal system with shift in the bands on the energy axis. (iii) A proper choice of metal (e.g., Ru) may exhibit ohmic nature in a graphene-inserted MoS_2-metal contact. These understandings would provide a direction in developing high-performance transistors involving heteroatomic layers as contact electrodes. © *2016 AIP Publishing LLC*.
[http://dx.doi.org/10.1063/1.4938742]

I. INTRODUCTION

Since the first demonstration of monolayer MoS_2-channel-based metal oxide semiconductor field effect transistor (MOSFET) by the EPFL research team,[1] the nanoelectronics community has shown tremendous interest towards 2D layered materials. These materials promise to offer exceptional electrostatic integrity and therefore are suitable for decananometer technology nodes.[2] However, the experimental reports of the drain current for such atomic layer channel-based MOSFETs are much lower than the desired ON current value required for technology downscaling. One of the primary reasons for such low ON current is inefficient carrier injection from the source to the channel, which originates from the significant Schottky barrier height (SBH) formed between the 2D channel material and the metal electrode (by SBH, we mean n-SBH unless it is specified elsewhere). Obtaining very low or even zero SBH at source/drain contacts is one of the most-essential and challenging tasks for realizing high-performance atomically-thin-material-based MOSFETs. Attempts are made to reduce SBH by choosing low-work-function metals (e.g., scandium,[3] molybdenum,[4] etc.) or even by employing low-pressure metal deposition techniques.[5] Novel doping methodology for TMD's[6–9] is also proposed to reduce the SBH. Very recently, it is demonstrated experimentally that, by inserting graphene layer between MoS_2 and metal electrode (Ti[10] and Ni[11]), SBH can be reduced significantly and hence greatly improve the drive current of the device. However, a detailed theoretical understanding of the underlying mechanism of such SBH reduction phenomena by inserting graphene layer is still lacking. It is also not clear if such technique successfully reduces SBH for the other metals commonly used as contact electrodes.

We utilize the density function theory (DFT) simulations to analyse the contact nature of the interfaces formed between monolayer MoS_2 and graphene-metal heterocontacts. The study is conducted for 5 different metals (Ti, Ag, Ru, Au, and Pt) which are commonly used in experiments, and the work function (WF) spans from low (Ti) to high (Pt) with an average interval of 0.25 eV. Both chemisorption and physiosorption interface metal surfaces with graphene are taken into account to develop better perception of the problem. We first simulate the MoS_2-graphene and graphene-metal systems separately and analyse their electronic structures. These understandings are then used to analyse the simulated characteristics of complex MoS_2-graphene-metal interface. To compare the SBH of a graphene-inserted system, the individual MoS_2-metal interfaces are also studied. A thorough examination of 16 different interface structures shows that SBH reduction through graphene insertion in a metal-MoS_2 contact is not always obtained for different metals. While we observe such reduction for Ti (in agreement with experiment), Ru, and Ag, an increase in SBH is observed in case of Au and Pt. It is further demonstrated that SBH in MoS_2-graphene-metal structure is governed by the property of graphene-adsorbed metal surface by analyzing the projected density of states (PDOS). The graphene insertion in a MoS_2-metal contact preserves the dispersion nature of the MoS_2 despite graphene-metal interface nature. Finally, we show by electron density difference (EDD)

investigation that choice of appropriate metal (as happens for Ru) may help to obtain pure ohmic contact in a MoS_2-graphene-metal system. It is worth noting that recent DFT studies on monolayer boron-nitride-inserted MoS_2-metal contact also reveal zero Schottky barrier nature with Co and Ni.[12]

II. COMPUTATIONAL DETAILS AND METHODS

DFT code as implemented in Atomistix Tool Kit (ATK)[13] employing local density approximation (LDA) with Perdew-Zunger parametrization (PZ)[14] as the exchange correlation functional is used for the present study. We first calculate the band gap of monolayer MoS_2 with the lattice parameter 3.1604 Å and found it to be 1.8 eV, which is consistent with the experimental studies.[15] Pseudopotentials conceptualized using the fully relativistic all-electron calculation[16] as developed by Hartwingster-Goedecker-Hutter (HGH) with tier 8 basis set are adopted for each element. The tier 8 basis set in ATK includes maximum number of atomic orbital contributions for HGH pseudopotential. We use such a higher basis set so that the dispersion of graphene-metal (especially graphene-gold[17]) and MoS_2-graphene interfaces[18] is persistent with the previous reports and thus assures the accuracy in the dispersion of complex MoS_2-graphene-metal systems. The iteration steps are set as 100 using Pulay mixer algorithm as the iteration control parameter with a tolerance value up to 10^{-5} Hartree. The Poisson solver we followed is fast Fourier transform (FFT). Density mesh cut off of 75 Hartree and a k point sampling of $9 \times 9 \times 1$ under Monkhorst Pack scheme for the Broiullin zone are chosen for the simulations. All the unit cells are relaxed using limited memory Broyden Fletcher Goldfarb Shannon method[19] until the forces on the atom are 0.01 eV/Å.

III. RESULTS AND DISCUSSIONS

A. Interface geometry

Keeping in mind the commensurability condition, the interface is formed by 4×4 MoS_2 supercell (lattice parameter = 12.6416 Å) and 5×5 graphene supercell (lattice parameter = 12.306 Å), and the mean strain on graphene is found to be 1.8%, which is in close agreement with earlier reports.[18] In the resultant structure comprising of graphene and MoS_2, it is observed that one S atom coincides with the carbon atom in graphene, respectively, forming TS configuration (C atom on top of S atom of MoS_2) as shown in Fig. 1(a) (top view). It is worth noting that, when the MoS_2 supercell is matched with graphene-metal heterocontact, the TS configuration between MoS_2 and graphene is not retained. This happens because the graphene is already interface matched with the metal slab and the atomic positions of carbon change with respect to metal. Hence, the MoS_2 atomic positions vary in accordance with the graphene-metal interface, which may be physiosorption or chemisorption. Figures 1(b) and 1(c) feature the overlap of carbon atom of graphene and the molybdenum and sulfur atoms of MoS_2 in a complex graphene-inserted MoS_2-metal interface for Ru (chemisorption) and Pt (physiosorption). For Ru, there is a close overlap of carbon atom with the underlying Mo and S atoms shown by black arrows. Both the Mo and S atom are located at the periphery of the hexagonal lattice. However, the overlap vanishes in case of Pt and there is no exact coincidence in the atomic positions for both the layers. This results due to variations in atomic positions of

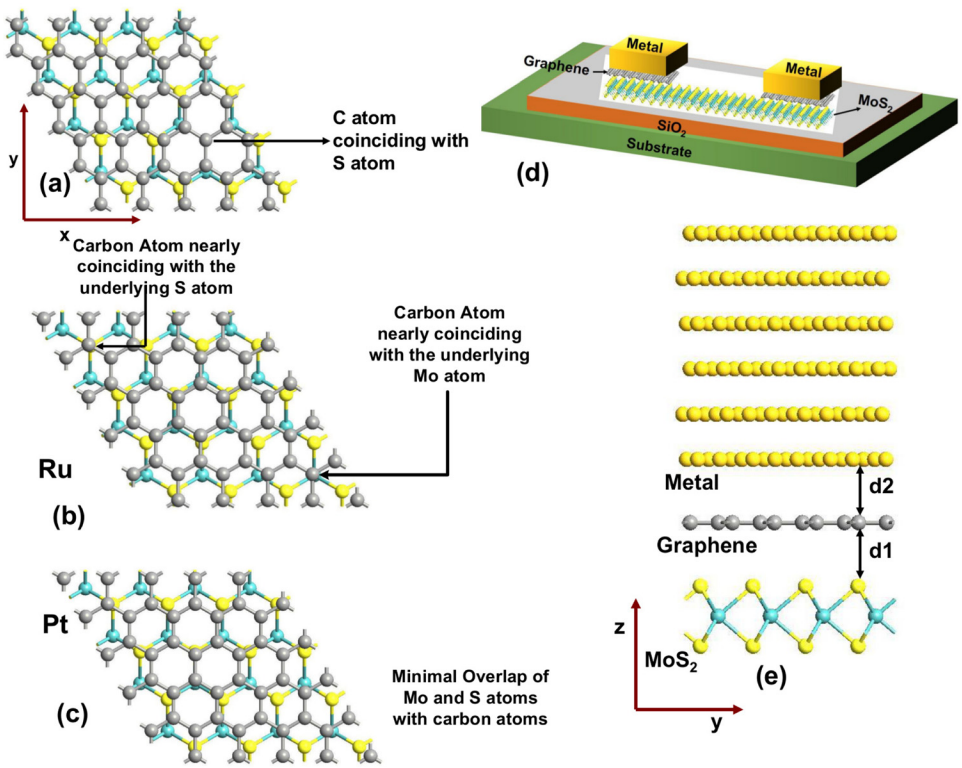

FIG. 1. (a) Top view of graphene (5×5 supercell) on MoS_2 (4×4 supercell) with equilibrium interlayer distance in a TS configuration (C atom on top of S atom of MoS_2). The grey, blue and yellow balls indicate carbon, molybdenum, and sulfur atoms, respectively. Variation in the overlap of Mo and S atoms of monolayer MoS_2 with carbon atoms of monolayer graphene for (b) MoS_2-graphene-Ru and (c) MoS_2-graphene-Pt. (d) Transistor schematic using graphene-metal heterocontact interfaced with monolayer MoS_2. (e) Side view of graphene-inserted MoS_2-Au contact with interlayer distance (z direction) corresponding to individual interface structures. The metal surface is cleaved along ⟨111⟩, and 6 atomic layers are used to make the interface. The atomic configurations are represented by Ball-Stick model.

MoS_2 supercell with respect to graphene-adsorbed metal interface and is different for different metals. The lattice of MoS_2 and graphene comes to a close equalization for 7×7 MoS_2 supercell (lattice parameter = 22.1228 Å) and 9×9 graphene (lattice parameter = 22.1508 Å) with a mean strain of 0.084%. To save the computational cost, for MoS_2-graphene and MoS_2-graphene-metal interface, we continued with the previous lattice parameter for the present analysis. ⟨111⟩ cleaved surface for Au, Ag, and Pt and ⟨0001⟩ cleaved surface for Ti and Ru, each with six layers, are interfaced and strained to match the supercells formed with monolayer graphene supercell and monolayer MoS_2 supercell and hetero-MoS_2-graphene interface.

Figure 1(d) shows the transistor schematic where the graphene layer is sandwiched between MoS_2 and metal for a top contact geometry used for the current study. The hybrid structure showing supercell formed using graphene-gold heterocontact and monolayer MoS_2 is presented in Figure 1(e). Table I provides the interface strain, equilibrium interlayer distance (d1 and d2), binding energies (BE), Dirac cone shift (ΔE_F), and the respective SBH for all the systems simulated in this work. The BE for MoS_2-metal and graphene-metal system is defined as following: BE (MoS_2/graphene-metal) = TE (MoS_2/graphene + metal) − TE (metal) − TE (MoS_2/graphene) and, for complex MoS_2-graphene-metal system, as BE(MoS_2-graphene-metal) = TE (MoS_2-graphene + metal) − TE (metal) − TE (MoS_2) − TE (graphene).

For a graphene-inserted MoS_2-metal interface, the distance between monolayer graphene-monolayer MoS_2 supercell (d1) and graphene-metal system (d2) is kept the same as the one obtained for individual interfaces. A distance of more than 20 Å is adopted in a perpendicular direction normal to the interface to isolate the slab from false interactions between periodic structures. Since both the 2D materials used have a hexagonal lattice parameter, so we have maintained the hexagonal lattice geometry for all the interface structures.

We first conduct DFT simulations on simple graphene interfaces such as MoS_2-graphene and graphene metal to study their dispersion natures. Further based on these characteristics, the electronic properties of complex MoS_2-graphene-metal systems are analyzed. The values of (ΔE_F) show that two metals (Ti and Ru) are chemisorped and 3 metals (Au, Pt, and Ag) are physiosorped with both graphene and MoS_2-graphene heterostructure. Apart from Pt, which is chemisorped with MoS_2, the rest of the metals show an interface nature with MoS_2 similar to graphene. The BE values confirm the kind of nature whether chemisorption or physiosorption for graphene, MoS_2, and MoS_2-graphene when interfaced with metals. For chemisorption interface, the values of BE are more negative in comparison to the physiosorped interface. From n-SBH values of MoS_2-metal and MoS_2-graphene-metal, we see that there is an increase in n-SBH for Au and Pt while a decrease is observed for the rest. The values of SBH show a minor change in a MoS_2-graphene-Au with respect to MoS_2-Au systems, thus confirming that graphene insertion in MoS_2-metal contact does not always ensure a SBH reduction. The same result is verified for Pt, where we see a significant increase of SBH value and shift in ΔE_F with graphene insertion with respect to graphene-Pt and MoS_2-Pt system. An increase in n-SBH implies a decrease of p-SBH, and it is more pronounced for Pt, while the other metals (Ag, Ti, and Ru) show an SBH reduction with Ru exhibiting the maximum decrease.

B. Electronic structure analysis

As been observed in earlier reports[20,21] for heterogeneous interfaces, obtaining the exact value of MoS_2 band gap and identification of VBM (valence band maxima) and CBM (conduction band minima) is difficult. Figure 2 shows the projected band structure and DOS of (a) MoS_2-Ru and (b) MoS_2-graphene-Ru interface. To determine the position of CBM and VBM in a MoS_2-metal interface, the projected band structure and PDOS of MoS_2 are kept alongside each other by aligning their Fermi level. The midgap states in DOS are very high for MoS_2-Ru (chemisorption interface) as compared to MoS_2-graphene-Ru interface because graphene acts as a buffer layer between MoS_2 and Ru. In a MoS_2-Ru interface, the VBM position is apparently visible, but the CBM position is ambiguous. The position of CBM is found out by measuring the band gap value from VBM position to an estimated CBM curvature, where the value is closer to 1.8 eV. To confirm these positions, DOS is placed beside and lines are drawn (black dotted lines), from CBM and VBM in band structure extending to the DOS region. In between this

TABLE I. Strain applied in all the interfaces, calculated equilibrium distances (z direction) corresponding to minimum binding energy (BE), BE values, Dirac cone shift only applicable to physiosorped interfaces involving graphene, Schottky barrier heights (p-type and n-type) corresponding to interfaces with MoS_2, and band gap (Eg) values for MoS_2-metal interface and MoS_2-graphene-metal interface calculated by adding p-type SBH and n-type SBH.

System	MoS_2-G	G-Au	G-Pt	G-Ti	G-Ag	G-Ru	MoS_2-Au	MoS_2-Pt	MoS_2-Ti	MoS_2-Ag	MoS_2-Ru	MoS_2-G-Au	MoS_2-G-Pt	MoS_2-G-Ti	MoS_2-G-Ag	MoS_2-G-Ru
Strain (%)	1.8	1.8	1.2	2.8	1.5	0.5	0.38	0.38	1.1	0.26	1.3	1.8	1.8	1.8	1.8	1.8
d (Å)	3.3	3.3	3.2	2.1	3.2	2.2	2.7	2.3	2.2	2.5	2.2	d1 = 3.3 d2 = 3.3	d1 = 3.3 d2 = 3.2	d1 = 3.3 d2 = 2.1	d1 = 3.3 d2 = 3.2	d1 = 3.3 d2 = 2.2
BE (eV)	−1.86	−2.5	−3	−19	−2.15	−5	−5.9	−9.55	−17.5	−6.5	−14.8	−4.5	−5.16	−23.81	−4.3	−12.43
ΔE_F	−0.02	0.1	0.28	—	−0.423	—	—	—	—	—	—	−0.106	0.127	—	−0.057	—
n-SBH	0.65	—	—	—	—	—	0.64	0.81	0.382	0.373	0.56	0.663	0.916	0.26	0.25	0.018
p-SBH	1.14	—	—	—	—	—	1.2	1.09	1.67	1.48	1.34	1.14	0.89	1.55	1.56	1.79
E_g (eV)	1.79	—	—	—	—	—	1.84	1.9	2.052	1.853	1.9	1.803	1.806	1.81	1.81	1.808

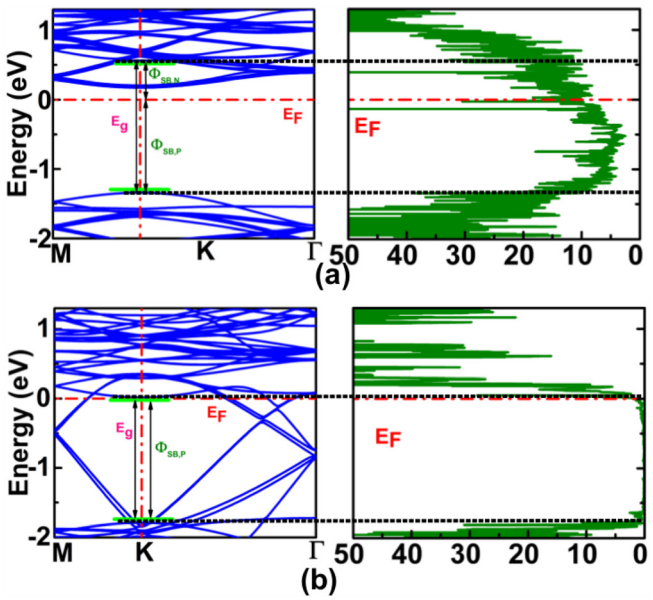

FIG. 2. Projected band structure and DOS of MoS_2 for (a) MoS_2-Ru interface and (b) MoS_2-graphene-Ru interface. Fermi level is positioned at zero and aligned to examine the positions of CBM and VBM.

particular interval, the midgap states contribution in DOS is minimal, which confirms the respective CBM and VBM positions. Depending on the type of interface (chemisorption and physiosorption), the amount of midgap states vary in the particular band gap regime. The variation in the MoS_2 band gap is higher for chemisorped interfaces as compared to physiosorped interfaces. The same methodology is used for MoS_2-graphene-metal interface and is shown for Ru metal (b). The difference is that the VBM position is not very precise, so the VBM position with respect to CBM is distinguished among various bands employing projected DOS. We see that the black dashed lines connecting the band edges in band structure with DOS connect perfectly at those energy levels where the contribution of PDOS is zero. Hence, in a graphene-inserted MoS_2-metal system, the band gap value remains closer to the pristine MoS_2 (1.8 eV). This shows that graphene layer acts as a perfect buffer between MoS_2 and metal and lessens the effect of metal on the band structure of MoS_2. In general, the chemisorption interfaces have higher midgap states in comparison to physiosorped interface due to high amount of hybridization at the interface. This makes the determination of CBM and VBM edges become difficult and is seen for other metals (Pd and Ir) as well.[21] The n-type SBH is calculated as E_C-E_F, and the p-type SBH is E_F-E_V and is shown by black arrows along with the conduction and valence band edges.

Figure 3 shows the projected band structure of carbon atoms for 5 × 5 graphene supercell for (a) MoS_2-graphene and (b)–(f) graphene-metal systems. The Dirac cone is preserved for only (a) MoS_2-graphene and for (b) graphene-gold, (c) graphene-platinum, and (e) graphene-silver interface with a shift with respect to E_F and is shown by black circles. This nature is completely lost for the chemisorption interfaces such as Ti and Ru. The shift of Dirac cone in graphene-Ag is higher and opposite in nature when compared to both Pt and Au. Figures 3(g)–3(l) show projected band structure of 4 × 4 MoS_2 supercell in a MoS_2-graphene interface (g) and graphene-inserted MoS_2-metal interface (h)–(l). A brown dashed line is drawn to identify the relative shift in CBM and VBM of MoS_2-graphene-metal systems with respect to the MoS_2-graphene system. The VBM and CBM are denoted by green lines. The CBM remains nearly same for MoS_2-graphene and MoS_2-graphene-Au systems, and it lowers down for Ti and Ag, but substantial shift is observed for Ru where CBM moves to the proximity of Fermi level. On the other hand, CBM shifts upwards for Pt. An ohmic nature appears for Ru contact, where we find n-type SBH to be almost zero (0.018 eV). The projected MoS_2 band structure nature of MoS_2-graphene is preserved for

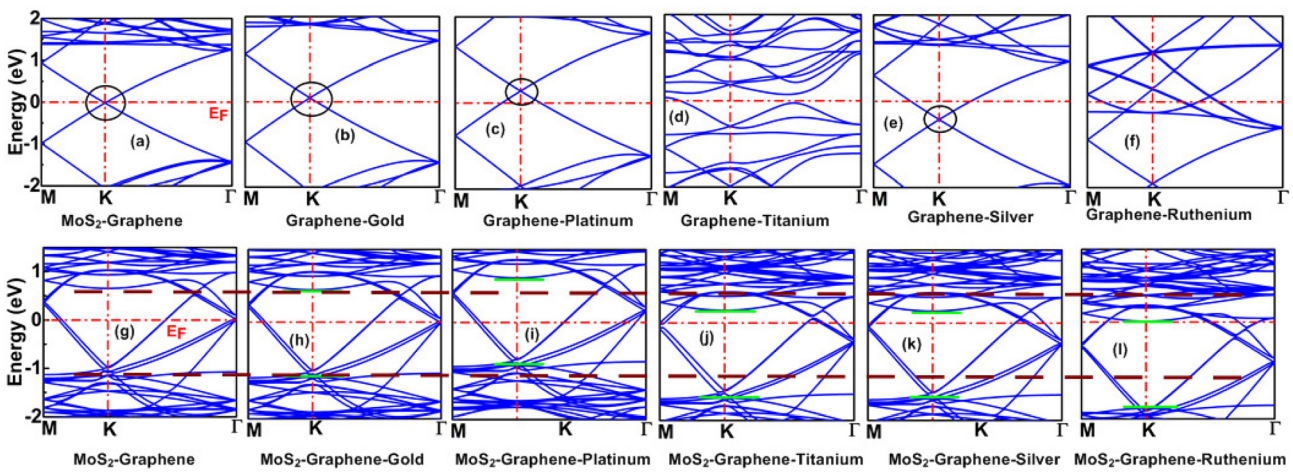

FIG. 3. Projected band structures of 5 × 5 graphene supercell for (a) MoS_2-graphene, (b) graphene-gold, (c) graphene-platinum, (d) graphene-titanium, (d) graphene-silver, and (d) graphene-ruthenium interface. For physiosorption cases (a), (b), (c), and (e), the Dirac cone is retained and indicated by black circles. For chemisorption cases (d) and (f), the Dirac cone is completely vanished. Projected band structures of 4 × 4 MoS_2 supercell for (g) MoS_2-graphene, (h) MoS_2-graphene-Au, (i) MoS_2-graphene-Pt, (j) MoS_2-graphene-Ti, (k) MoS_2-graphene-Ag, and (l) MoS_2-graphene-Ru interface. Since the midgap states are present in the heterogeneous interface, the valence band maxima (VBM) and conduction band minima (CBM) are presented by green lines. The brown dashed lines are aligned with the CBM and VBM of projected MoS_2 of MoS_2-graphene interface in (g) and highlight the variation of respective CBM and VBM of other interface structures. The Fermi level is denoted by E_F and is set as zero.

every MoS_2-graphene-metal interface, and the interface states are found to be minimal. This again implies that graphene is successful in isolating the MoS_2 from metal with nearly equivalent zero midgap states and only shifts of CBM and VBM with respect to MoS_2-graphene system, and the graphene-metal interaction dictates the amount and nature of shift.

C. Density of states analysis

The relative shift of MoS_2 band edges and perturbation in the Dirac nature among various MoS_2-graphene-metal interfaces are highlighted in Figure 4 using the PDOS. Figures 4(a)–4(e) and 4(f)–4(j) show the PDOS of 4 × 4 MoS_2 supercell and 5 × 5 graphene supercell, respectively. We superimpose the PDOS of MoS_2-graphene system over the MoS_2-graphene-metal system to present the difference in amounts of hybridization for physiosorped and chemisorped metals. The p-orbital of carbon in graphene and d-orbital of Mo, which are maximum contributors for the Dirac cone in graphene[22] and VBM, CBM positions in MoS_2,[23] respectively, are used to study these effects. In Figures 4(a)–4(e), we see the relative shifts in the Mo-d orbital edges for various metals. They are consistent with the projected band structure shown in Figures 3(g)–3(l). In terms of hybridization, it is observed that, in the weakly chemisorped metal Pt (4(b)) and highly chemisorped metal Ti and Ru (4(c) and 4(e)), the CB and VB edges are highly perturbed in comparison to Au and Ag (4(a) and 4(d)) From Figure 4(f), it is seen that carbon p orbital contribution of MoS_2-graphene and MoS_2-graphene-Au are nearly similar to each other since graphene is physiosorped on MoS_2 and Au and hence the Dirac nature is least perturbed. This nature of perturbation is observed in Ag and Pt as well, and the Dirac cone gets shifted from the zero point Fermi level as compared to MoS_2-graphene system. When we compare the ΔE_F in graphene-metal with MoS_2-graphene-metal from Table I, we see that the change in ΔE_F is highest for Ag when contacted with MoS_2-graphene system, and hence, the SBH reduction is also maximum for Ag for all physiosorped metals. The variation of Pt is higher as compared to Au since Pt has one electron less in d-orbital as compared to Au, so it's more reactive. The nature of shift for Au and Pt also are opposite as compared to Ag, and hence, we see SBH reduction for Ag and SBH increment for both Au and Pt. For chemisorped metal Ti and Ru, the Dirac nature is completely lost. The interlayer separation between graphene and Ti/Ru is much less in comparison to Au, Ag, and Pt; hence, we see higher interface states near the Fermi level for Ti and Ru. This is indicative of strong and complex bonding between the carbon and metal atoms. Ti being the d-electron metal has a completely filled s-orbital, thus is more reactive. It is chemisorped with graphene and MoS_2, so the perturbations in the orbitals are very high as compared to Au and reflect a complete distortion. Thus, we see SBH alterations for MoS_2-graphene-Ti with respect to MoS_2-graphene. In case of Ru, both d and s orbitals are partially filled and the perturbations for carbon-p lie intermediate between the two cases, i.e., Au and Ti. Thus, it is expected that its chemical reactivity also follows the same trend. But the change in SBH in Ru is higher as compared to Ti, which is further understood by electron density difference.

From the Mo-d orbital contribution in PDOS, we observe that, for Au, they exactly overlap each other, which implies that MoS_2 band structure is least affected. This is due to the minimum interaction between graphene-Au interfaces. However, for Ru and Ti, the electronic structure of graphene is highly perturbed, so Mo d-orbital experiences a shift with respect to MoS_2-graphene interface. The amount of shift is further examined using the EDD analysis.

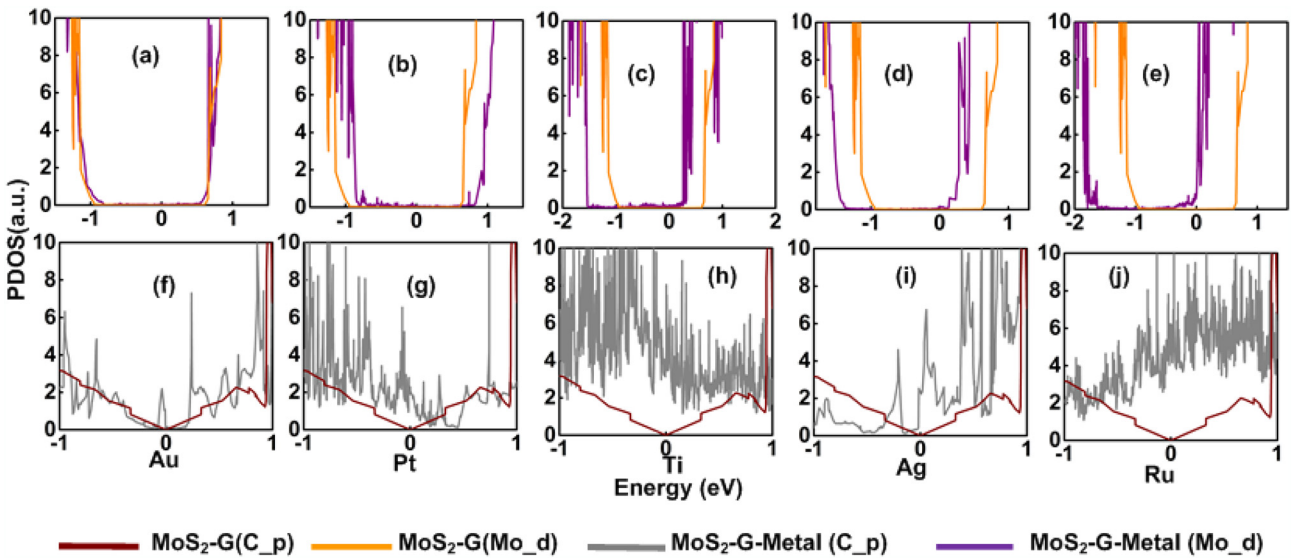

FIG. 4. Projected density of states of Mo-d orbital and C-p orbital MoS_2-graphene-metal heterocontacts interfaces for (a) and (f) Au, (b) and (g) Pt, (c) and (h) Ti, (d) and (i) Ag, and (e) and (j) Ru systems superimposed with that MoS_2-graphene system. The legends are specified at bottom. The shifts in the orbitals of complex MoS_2-graphene-metal are compared w.r.t the MoS_2-graphene interface.

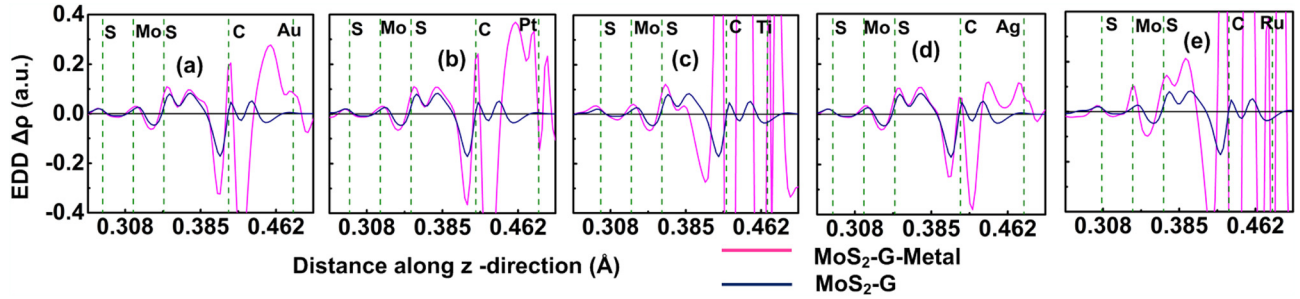

FIG. 5. Electron density difference (EDD) for (a) MoS_2-G-Au, (b) MoS_2-G-Pt, (c) MoS_2-G-Ti, (d) MoS_2-G-Ag, and (e) MoS_2-G-Ru system superimposed with EDD of MoS_2-graphene systems. The EDD values on the y-axis are scaled by a factor of 10^3.

D. Charge transfer investigation

The shifts observed in CBM/VBM and the amount of perturbations in the orbital contribution are further explored by evaluating the EDD averaged along z direction shown in Figures 5(a)–5(e). For MoS_2-graphene-metal interface, the EDD is calculated as $\Delta\rho = \rho_{MoS_2+graphene+metal} - \rho_{MoS_2} - \rho_{graphene} - \rho_{metal}$, where ρ is the electron density. The EDD of MoS_2-graphene interface is superimposed on the top of MoS_2-graphene-metal interface in order to develop better understandings of charge transfer occurring at MoS_2-graphene-metal interface. While comparing EDD with respect to MoS_2-graphene interface, the perturbation in Ti and Ru is very high as compared to Au, Ag, and Pt at the interface of carbon and interacting sulfur atom of MoS_2 since Ti and Ru are chemisorped with graphene. Both charge accumulation and depletion regions are found at the interface and, depending on the metal, these vary for the different interfaces. This leads to charge distribution and further dipole formation at the interface, which results in band alignment.[24] We calculate the area under the EDD curve between the nearest sulfur atom and the carbon atoms to analyse the shift in VBM and CBM.[25] Table II shows the value calculated for MoS_2-graphene-metal structures for different metals. Positive values imply a higher accumulation region with more chemical interaction at the interface, while negative values imply the opposite. Negative values are obtained only for Au and Pt and are higher for Pt. This depicts there is minimal charge transfer from Pt to MoS_2-graphene system and surface charge repulsion for both Au and Pt. Hence, we find an increase in n-SBH for Au and Pt systems. On the other hand, for Ag, Ti, and Ru, the area obtained is positive, which leads to more accumulation as compared to depletion. The maximum area obtained is for Ru, and so we observe a maximum decrease of SBH.

TABLE II. Area calculated between the interfacial sulfur atom of MoS_2 and carbon atom of graphene for various MoS_2-graphene-metal interfaces.

System	Area under EDD between C and S atoms
MoS_2-G	1.7×10^{-7}
MoS_2-G-Au	-1.04×10^{-7}
MoS_2-G-Ag	3.42×10^{-7}
MoS_2-G-Ti	5.62×10^{-6}
MoS_2-G-Pt	-3×10^{-7}
MoS_2-G-Ru	8.1×10^{-6}

E. Work function calculation and Fermi level pinning

We calculate the WF of bare and graphene-adsorbed metals using the ghost atom technique,[26] which helps to extend the basis set in the vacuum region. The work function values obtained are 6.05 eV, 5.51 eV, 5.48 eV, 4.82 eV, and 4.66 eV for Pt ⟨111⟩, Au ⟨111⟩, Ru ⟨0001⟩, Ag ⟨111⟩, and Ti ⟨0001⟩ surfaces, respectively. They are in near equivalence with the experimental values of those particular surfaces.[27] For graphene-adsorbed metal, the value changes to 4.93 eV, 4.7 eV, 3.47 eV, 4 eV, and 4.21 eV for Pt, Au, Ru, Ti, and Ag, which are consistent with the earlier reports.[22] The WF of free-standing MoS_2 and graphene are found to be 5.2 eV and 4.56 eV.

We see a correlation between the change of the SBH of a MoS_2-metal system due to graphene insertion and the work function modulation of the metal due to graphene adsorption. The maximum reduction in WF is seen for ruthenium, and hence, we observe large reduction in n-SBH for Ru as well. Figure 6(a) shows the variation of SBH for MoS_2-metal and MoS_2-graphene-metal interface with respect to the metal WF. The SBH of MoS_2-graphene with a value of 0.65 eV is shown by a blue line and acts as the reference to study the alteration of SBH. We see the trend obtained in MoS_2-metal is different from the trend obtained in MoS_2-graphene-metal, where the main deviation arises for Ru. Figure 6(b) features the variation of SBH of MoS_2-metal interface and MoS_2-graphene-metal interface with respect to WF_{Metal}-WF_{MoS_2} and $WF_{graphene-metal}$-WF_{MoS_2}, respectively. The SBH has a linear dependence with a value of 0.61 for MoS_2-graphene-metal and 0.31 for MoS_2-metal interface. Fitting these characteristics with a linear equation yields in increase of slope from 0.31 to 0.61 due to graphene insertion. Hence, it could be inferred that graphene insertion helps to de-pin the Fermi level partially in a MoS_2-metal interface.

In the above discussion, we explain the underlying mechanism of SBH change of the MoS_2-graphene interface, when a metal slab is placed beneath the graphene. However, it is difficult to conceive similar explanation for the change of SBH with respect to the MoS_2-metal interface. This is because the contact nature of the MoS_2-graphene-metal system is dictated by the graphene-metal interaction, which is

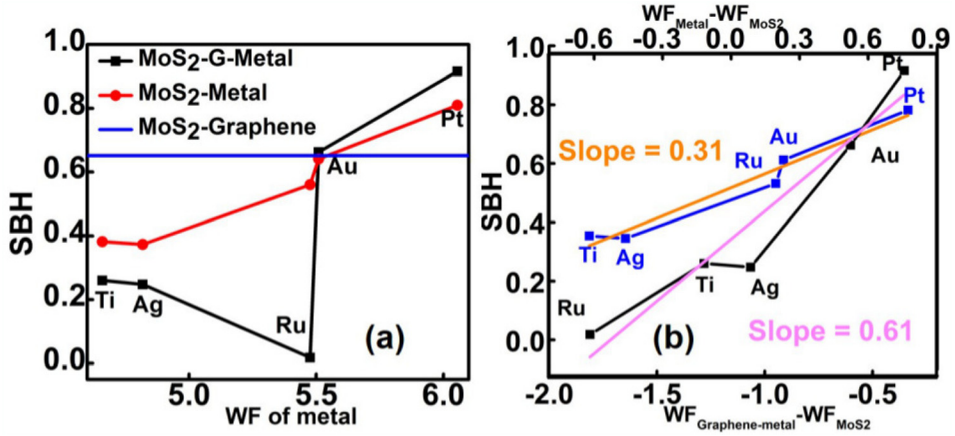

FIG. 6. (a) Plot highlighting comparison of SBH of MoS_2-metal and MoS_2-graphene-metal interface with respect to the work function of various metals. The SBH for MoS_2 obtained with MoS_2-graphene system is shown by blue line depicting the increase and decrease of SBH of metals in MoS_2-graphene-metal systems. (b) Dependence of MoS_2-metal SBH (blue line) versus WF_{Metal}-WF_{MoS_2} and MoS_2-graphene-metal SBH (black line) versus $WF_{graphene-metal}$-WF_{MoS_2} for all the metals. The orange and pink lines show the linear fitting of the two curves.

very different from the nature of interaction observed in MoS_2-metal interface.

IV. CONCLUSION

In conclusion, we have conducted rigorous DFT calculation to investigate the charge transfer from metal to MoS_2 in a graphene-inserted MoS_2-metal contact involving five different metals (Ti, Ag, Ru, Au, and Pt). Graphene acts as a perfect buffer separating MoS_2 from metal and thus retains the band gap nature with minimal interface states. Different metals showed varying behavior, and inserting graphene in a metal MoS_2 contact does not assure a SBH reduction. An increase in SBH is observed for Au and Pt while a decrease for Ag and Ti, and an ohmic nature is found for Ru. A large fluctuation in the band alignments is due to the interface charge transfer, which further leads to the dipole formation. The variation observed in SBH is highly dependent on the nature of the graphene-metal interface. These findings can lead to further design of high-performance transistors using heterostructures as contacts.

ACKNOWLEDGMENTS

The work was supported by the Science Engineering and Research Board, Department of Science and Technology, Government of India, under Grant SR/S3/EECE/0151/2012.

[1]B. Radisavljevic, A. Radenovic, J. Brivio, V. Giacometti, and A. Kis, Nat. Nanotechnol. **6**, 147 (2011).
[2]See http://www.itrs.net/ for ITRS.
[3]S. Das, H.-Y. Chen, A. V. Penumatcha, and J. Appenzeller, Nano Lett. **13**, 100 (2013).
[4]J. Kang, W. Liu, and K. Banerjee, Appl. Phys. Lett. **104**, 093106 (2014).
[5]C. D. English, G. Shine, V. E. Dorgan, K. C. Saraswat, and E. Pop, in *72nd Annual Device Research Conference (DRC)* (IEEE, 2014), pp. 193–194.
[6]L. Yang, K. Majumdar, H. Liu, Y. Du, H. Wu, M. Hatzistergos, P. Y. Hung, R. Tieckelmann, W. Tsai, C. Hobbs, and P. D. Ye, Nano Lett. **14**, 6275 (2014).
[7]J. Suh, T.-E. Park, D.-Y. Lin, D. Fu, J. Park, H. J. Jung, Y. Chen, C. Ko, C. Jang, Y. Sun, R. Sinclair, J. Chang, S. Tongay, and J. Wu, Nano Lett. **14**, 6976 (2014).
[8]M. R. Laskar, D. N. Nath, L. Ma, E. W. Lee, C. H. Lee, T. Kent, Z. Yang, R. Mishra, M. A. Roldan, J.-C. Idrobo, S. T. Pantelides, S. J. Pennycook, R. C. Myers, Y. Wu, and S. Rajan, Appl. Phys. Lett. **104**, 092104 (2014).
[9]H. Fang, S. Chuang, T. C. Chang, K. Takei, T. Takahashi, and A. Javey, Nano Lett. **12**, 3788 (2012).
[10]Y. Du, L. Yang, J. Zhang, H. Liu, K. Majumdar, P. D. Kirsch, and P. D. Ye, IEEE Electron Device Lett. **35**, 599 (2014).
[11]W. S. Leong, X. Luo, Y. Li, K. H. Khoo, S. Y. Quek, and J. T. Thong, ACS Nano **9**, 869 (2015).
[12]M. Farmanbar and G. Brocks, Phys. Rev. B **91**, 161304 (2015).
[13]See http://quantumwise.com/ for Atomistix ToolKit v.14.1 Quantumwise.
[14]J. P. Perdew and A. Zunger, Phys. Rev. B **23**, 5048 (1981).
[15]K. F. Mak, C. Lee, J. Hone, J. Shan, and T. F. Heinz, Phys. Rev. Lett. **105**, 136805 (2010).
[16]C. Hartwigsen, S. Goedecker, and J. Hutter, Phys. Rev. B **58**, 3641 (1998).
[17]J. Sławińska, P. Dabrowski, and I. Zasada, Phys. Rev. B **83**, 245429 (2011).
[18]Y. Ma, Y. Dai, M. Guo, C. Niu, and B. Huang, Nanoscale **3**, 3883 (2011).
[19]See https://wiki.fysik.dtu.dk/ase/ase/optimize.html#module-ase.optimize.lbfgs for LBFGS.
[20]W. Chen, E. J. Santos, W. Zhu, E. Kaxiras, and Z. Zhang, Nano Lett. **13**, 509 (2013).
[21]C. Gong, L. Colombo, R. M. Wallace, and K. Cho, Nano Lett. **14**, 1714 (2014).
[22]P. A. Khomyakov, G. Giovannetti, P. C. Rusu, G. Brocks, J. van den Brink, and P. J. Kelly, Phys. Rev. B **79**, 195425 (2009).
[23]C. Gong, H. Zhang, W. Wang, L. Colombo, R. M. Wallace, and K. Cho, Appl. Phys. Lett. **103**, 053513 (2013).
[24]R. T. Tung, Phys. Rev. B **64**, 205310 (2001).
[25]A. Chanana and S. Mahapatra, IEEE Trans. Electron Devices **62**, 2346 (2015).
[26]See http://quantumwise.com/publications/tutorials/item/499-computing-the-work-function-of-a-metal-surface-using-ghost-atoms for calculating the work function of metals with ghost atom technique.
[27]D. R. Lide, editor, *CRC Handbook of Chemistry and Physics*, Internet Version 2005, http://www.hbcpnetbase.com (CRC Press, Boca Raton, FL, 2005).